Liquid Metal-Enabled Filtering Switches and Switchplexers

Wu, Yi Wen; Qian, Lu; Churm, James; Wang, Yi

DOI:
10.1109/TMTT.2024.3357968

Liquid Metal-Enabled Filtering Switches and Switchplexers

Yi-Wen Wu, *Member, IEEE*, Lu Qian, *Member, IEEE*, James Churm, Yi Wang, *Senior Member, IEEE*

***Abstract*—The via-pad-slot (VPS) structure, as the switchable element, has been used to demonstrate a single-pole-triple-throw (SPTT) filtering switch and a switchplexer. The VPS can be flexibily switched by using liquid metal (LM) or high dielectric constant materials to either cover or uncover the slot. Since the LM only moves on the surface of the VPS and the SIW, the implementation and actuation of the LM is simple and does not cause excessive loss on the device. In the switchplexer design, all channels can be switched ON and OFF to form filters or multiplexers of various channel combinations. Additional transmission zeros can be generated by the loaded, partially switched-OFF channel. The generation of the transmission zeros was discussed and analyzed using coupling matrix approach. The demonstrated X-band (9.56-10.44 GHz) cross-shaped SPTT 5th-order filtering switch exhibits a suppression level of better than 40 dB at 8 and 12 GHz, an insertion loss of 1.55 dB at 10 GHz, and an isolation level of 58 dB at 10 GHz. The X-band switchplexer operates at three frequency bands, e.g., 11.08-11.55 GHz, 10.61-10.99 GHz, and 9.76-10.33 GHz. The LM-enabled VPS-based switchable element can be integrated with other multifunctional circuits and systems for channel control and reconfiguration.**

***Index Terms*— Coupling matrix, filtering switch, liquid metal, switchable element, switchplexer, transmission zeros.**

I. INTRODUCTION

RECONFIGURABLE or tunable devices have been in high demand from the rapid development of compact multifunctional front-end systems [1], [2], [3]. A key component is a switch with excellent linearity, low insertion loss (IL), and high power handling [4]. PIN diodes and varactors have been extensively used in such reconfigurable devices, [5], [6], [7], [8], [9], [10], [11], [12]. However, most of them suffer from high IL, nonlinearity, low power handling, and limited bandwidth. Despite low power handling, microelectromechanical systems (MEMS) switches have distinct advantages in their high linearity, low IL, and wide bandwidth compared to PIN diodes [4], [13], [14], [15], [16], [17]. While MEMS switches are compact, implementing a significant quantity of switches still faces challenges in terms of reliability and cost.

Gallium (Ga)-based liquid metals (LM) alloys, e.g., Galinstan and EGaIn, are conductors of unique properties of low melting points, fluidity, and high electrical conductivity [18], [19], [20]. They have been explored for use in 'mechanical-style' switches. LM-based MEMS switches have been studied in [21], [22], [23], [24] to reduce the contact resistance and therefore IL. In [21], Galinstan is placed in a microfluidic channel filled with Teflon solution, and moved by external pressure to change the state of a coplanar waveguide (CPW) line. The measured IL of the switch is 0.2 – 1.3 dB from 20 to 100 GHz, and the isolation is better than 20 dB. In [22], the LM is actuated by continuous electrowetting (CEW) by modifying the surface tension of the LM immersed in NaOH solution. When the LM is moved over the CPW, the isolation is better than 10 dB from dc to 11 GHz. When the air bubble is moved to replace the LM, the IL ranges from 0.2 to 3 dB within dc-11 GHz. Note that the use of NaOH solutions may lead to additional IL. To avoid this, LM can be actuated by electrowetting on dielectric (EWOD) [23], [24] when the surface tension and contact angle of the LM can be manipulated by applying electric fields. The demonstrated IL is better than 0.3 dB, and the isolation is better than 20 dB over dc-40 GHz [23]. A LM-based waveguide switch is reported in [25], where the EGaIn and Hydrocal 2400 oil are injected into the PTFE tube. By inserting/removing the tube into/from the waveguide, the switch can be turned OFF and ON. The IL is 0.1 dB and isolation is better than 30 dB at 20 GHz. Substrate-integrated waveguide (SIW) has been widely used in microwave circuits due to its ease of integration and low loss. In [26], a removable wall of a SIW is realized by a row of drill holes. When they are filled with LM, it operates in the "OFF state" and the isolation is better than 30 dB from 2.4 to 4.3 GHz. When the LM is emptied from the holes, it operates in the "ON state" and the IL is better than 0.5 dB. However, the actuation method is cumbersome, so it is difficult to apply to high frequency band and integration.

Filters and switches are usually cascaded separate components in many RF systems. This may lead to performance degradation due to interstage mismatching [27]. Filtering switches integrate the functions of switches [4], [28] and filters [29], and have attractive features for miniaturized, multifunctional circuits and systems. Most filtering switches are based on PIN diodes [30], [31], [32], [33]. In [30], a 2nd-order microstrip single-pole-single-throw (SPST) filtering switch was proposed. The achieved IL at 0.9 GHz is 3 dB, the suppression level is only 20 dB at 0.66 GHz, and the isolation is 41 dB at 0.9 GHz. [31] also reported a 2nd-order SPST filtering switch with lumped capacitors and a PIN diode.

Manuscript received Month DD, YYYY; revised Month DD, YYYY; accepted Month DD, YYYY.

This work was supported by UK Engineering and Physical Sciences Research Council grants EP/V008382/1. For the purpose of open access, the author(s) has applied a Creative Commons Attribution (CC BY) license to any Accepted Manuscript version arising. (Corresponding author: Lu Qian)

Y. Wu, L. Qian, J. Churm, and Y. Wang are with School of Engineering, University of Birmingham, B15 2TT, United Kingdom (e-mail: y.wu.7@bham.ac.uk, l.qian.1@bham.ac.uk; j.r.churm@bham.ac.uk; y.wang.1@bham.ac.uk).

When the diode is OFF, the switch is ON with an IL of 1.8 dB at 0.78 GHz and 20-dB suppression within 0.89-5.3 GHz [31]. When the diode is ON, the signals through two transmission paths between port1 and port2 are cancelled out to OFF-state, where the isolation is higher than 28 dB within 0.75-0.82 GHz [31]. In [32], a 3rd-order single-pole-double-throw (SPDT) filtering switch was realized using PIN diodes and multi-coupled lines. The IL is less than 0.97 dB within 0.95-1.05 GHz, the stopband rejection is better than 25 dB at 4 GHz, and the isolation level between the two output ports is better than 40 dB [32]. [33] reported a 4th-order coupled-resonator SPDT filtering switch, with an IL of 3.6 dB at 1.49 GHz, suppression of 27 dB at 15 GHz, and isolation of 47 dB at 1.49 GHz. Based on the varactor-loaded SIW and piezo, a 3rd-order SPDT was reported [34]. The IL of the SPDT is around 3.1 dB within 1.956-2.782 GHz, and the suppression and isolation levels are 45 and 47 dB, respectively. In [35], a 4th-order SPDT filtering switch consisted of tunable non-resonating nodes and varactor-loaded microstrip resonators. The IL is about 6.73 dB within 1.65-1.84 GHz, and the suppression and isolation levels are 32.5 and 40 dB, respectively. [36] introduced a 3rd-order single-pole-four-throw (SP4T) filtering switch with a P-I-N diodes loaded tri-mode resonator. The IL is about 1.76 dB at 0.99 GHz, the suppression level is 38 dB, and the isolation level is 45.7 dB. All these filtering switches are at low frequency and show relatively high IL.

In [37], a waveguide single-pole-triple-throw (SPTT) filtering switch is realized by using tuning pins. When the pin is fully inserted into the waveguide, the detuned filter works at its OFF state. When the pin is extracted, the tuned filter works at ON state. Low IL of 0.31 dB was achieved at 12 GHz. The suppression is about 28 dB at 13 GHz, and the isolation is better than 50 dB within 11-13 GHz [37]. The use of waveguide structure and pins make the device bulky, which may be undesirable for high integration circuits and systems.

As an attempt to overcome these challenges, we have demonstrated two switching devices using a novel switchable element, the so-called via-pad-slot (VPS) structure, enabled by gallium-based liquid metals (LMs). An X-band cross-shaped SPTT filtering switch and a three-channel switchplexer are presented. The operation mechanism of the switchable element is explained in Section II. The theories and designs of the filtering switches and the switchplexer are introduced in Section III and Section IV, respectively. Then Section V shows the fabricated prototypes and measured results. Finally, Section VI draws a conclusion.

II. Principle of Operation

A. Switchable Element - the Via-Pad-Slot (VPS) Structure

To facilitate planar actuation of LM in a SIW structure, we have used a switch component designed on the surface of the SIW. As shown in Fig. 1, this crucial component used here is a via-pad-slot (VPS) structure, consisting of a via, a pad, and an annular slot that isolates them from the ground. The via is connected to the lower ground of the SIW. As presented in Fig. 1(a), when the VPS structures are inserted in a SIW

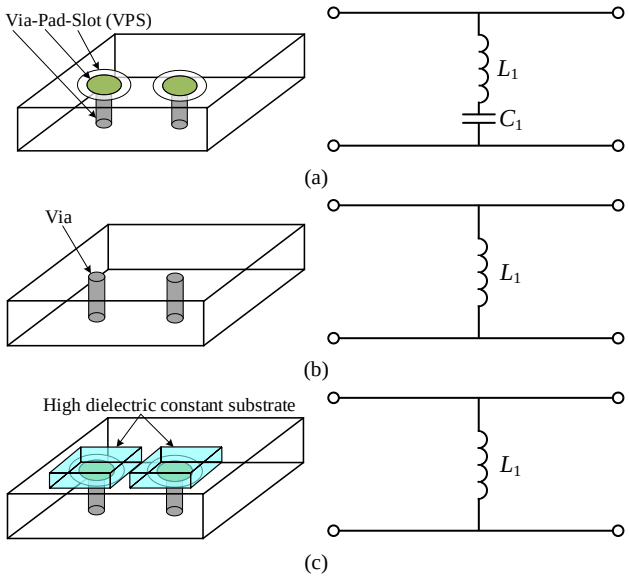

Fig. 1. States and equivalent circuits of the switchable element. (a) ON state (VPS structure). (b) OFF state (VPS covered by LM). (c) OFF state (VPS covered by high dielectric constant substrate).

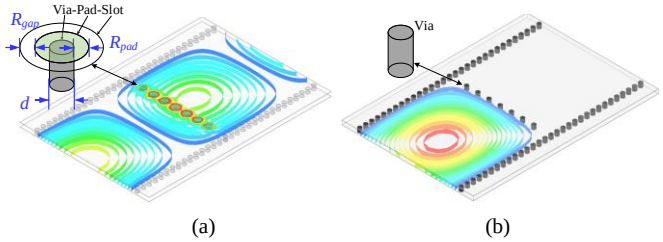

Fig. 2. Configuration and electric field distributions of a SIW switch with VPS structures. (a) ON state. (b) OFF state.

structure, its equivalent circuit is a shunt inductance (L_1) and a capacitance (C_1) [20]. When the slot of the VPS is covered by LM, the via and pad are shorted to the ground. The VPS structure is switched to a normal metal via, and the shunt capacitance disappears, as illustrated in Fig. 1(b). This VPS structure transfers the switching component from the inside of the SIW [38] to the surface, which avoids the complexity of injecting and emptying LM in the vertical holes. This not only simplifies the actuation of the LM, but also improves the integration. Even more importantly, the IL is reduced by avoiding the loss associated with the LM inside the SIW.

Apart from the LM, high dielectric constant material can also be used to exert switching. In Fig. 1(a), the equivalent capacitance C_1 is associated with the slot between the pad and the ground on the upper surface of the SIW. C_1 can be estimated by $C_1 = \varepsilon_0(\varepsilon_1 + 1)S/2d$, where S is the equivalent area of the "parallel plate" capacitor, d is the distance between the pad and the ground, ε_0 is the vacuum permittivity, and ε_1 is the relative dielectric permittivity of the SIW substrate. As shown in Fig. 1(c), when the VPS structure is covered by a very high dielectric constant (high-k) material, e.g. distilled water (ε_r = 81) or Barium lanthanide tetratitanates (BLT, ε_r = 200) [39], C_1 may become very large. Its impedance Z ($= 1/j\omega C_1$) diminishes, equivalent to a short circuit. It will be demonstrated later that a high-k material could also be used to switch the states of the VPS structures.

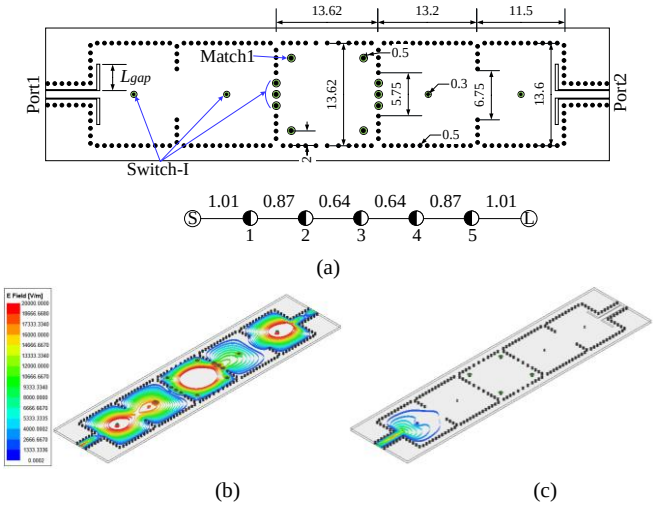

(a)

(b) (c)

Fig. 3. SPST 5-pole filtering switch. (a) Configuration. Electric field distributions of (b) ON state and (c) OFF state.

B. SIW Switch Based on VPS Structure

Since the equivalent circuit of a VPS structure is a shunt inductance-capacitance, the electromagnetic (EM) signal may pass through a row of VPSs as shown in Fig. 2(a). This is the "ON state", and the simulated insertion loss at the ON state is 0.29 dB at 10 GHz. When the VPSs are covered by the LM or high-*k* dielectrics, the rows are transformed into shorting vias, hindering the transmission as demonstrated in Fig. 2(b). The isolation at the OFF state is 34 dB at 10 GHz. This shows the mechanism to alter the operating states. For the peristaltic pump-based actuation method used in this work, the measured flow rate of the peristaltic pump is 20 mm^3/s. Considering the width and height of the microfluidic channel is 1.2 mm and 1 mm, respectively, the movement speed of LM is 16.67 mm/s. As the width of the SIW is 13.6 mm, the switching time of the VPS-based SIW switch illustrated in Fig. 2 is estimated at about 0.82 s. For each VPS, the estimated switching time is approximately 0.06 s. The distance between the edge of the pad and the edge of the via is 0.13 mm, and the width of the slot is 0.13 mm. In this work, all the designs are simulated by Ansys Electronics Premium HFSS, and all the VPSs have the same R_{pad} and R_{gap}, and the only difference in the VPS structures is the diameter of the via. When such VPSs are used with resonators in a filter, a filtering switch may be formed as will be discussed next.

III. Design of Filtering Switch

A. Single-Pole-Single-Throw Filtering Switch

As mentioned in Section II-B, the VPS structure can be designed not to affect the transmission of RF signal. Therefore, the design methods for a conventional SIW filter remain applicable to the filters with VPS structures. A X-band, 5th-order, single-pole-single-throw (SPST) filtering switch is first designed. The design and the mathematical formation involved can be found from textbooks such as [40]. The substrate is Taconic TLY-5 with a thickness of 0.508 mm, dielectric constant of 2.2, and loss tangent of 0.0009. The width (W_{wg}) of the standard WR90 waveguide is 22.86 mm, so the original width (W_1) of the X-band SIW can be calculated by (1)

$$W_1 = \frac{W_{wg}}{\sqrt{\varepsilon_r}} \tag{1}$$

As marked out in Fig. 3(a), there are two types of VPS structures. The 'Switch-I' type is designed to turn ON/OFF the filter. Such VPSs are placed in the middle of the resonators and across the iris between two adjacent resonators. When the LM (EGaIn, $\sigma = 3.4 \times 10^6$ S/m [19]) is not loaded, the filter operates at the "ON state", and the EM field distribution is shown in Fig. 3(b). When the 'Switch-I' VPSs are covered by the LM, they become shorting vias and block the transmission. The EM field distribution corresponding to this OFF state is shown in Fig. 3(c). The other types of VPSs are marked out as 'Match1' in Fig. 3(a). They are located at the four corners of the central resonant cavity, designed for impedance matching in a single-pole muti-throw switch. This will be discussed later. The key dimensions are given in Fig. 3(a).

With the VPS structures, additional shunt inductance and shunt capacitance are introduced. This further reduces the overall size of the SIW. The optimized W_1 is 13.6 mm.

Since both the thickness of the substrate and the size of the VPS structure are much smaller than the wavelength, the parallelly introduced equivalent inductance and capacitance from the VPS structure can be disregarded. Hence, the influence of the VPS structure on the filter design is negligible. This implies that the conventional SIW filter design method can be applied to the design of the filtering switch with the VPS structure.

Herein, the design of the 5th-order SPST filtering switch (f_0 = 10 GHz, FBW = 8.8%) is detailed as an example. All the circuits shown in this work follow the same design process. It starts from obtaining the coupling coefficients by calculation according to the filter specification, as illustrated in Fig. 3(a). The practical physical structure of the filtering switch will be determined following the simulation-based dimensioning procedure [40]. The full-wave electromagnetic simulation software Ansys Electronics Premium HFSS is used. Fig. 4 shows all extracted design curves (including resonance frequency, coupling coefficients) for this design example, where both cases with/without VPS structure are considered.

The dimensions of the resonators are related to their resonating frequencies. Shown in Fig. 4(a) are the resonating frequencies of the rectangular cavities with/without VPS structure as a function of the length (L_1), where the width (W_1) of the SIW remains unchanged at 13.6 mm. It is evident that the VPS structure has little effect on the resonating frequencies. When the VPS is inserted into the normal rectangular cavity (W_1 = 13.6 mm, L_1 = 13.25 mm), the fractional frequency deviation is only 1.1%. Hence, the resonant frequency of the cavity with VPS structure can be approximately calculated using the formula (2) of the traditional rectangular resonant cavity. For a more accurate estimate, formula (3) takes the frequency offset into consideration.

$$f_{Normal} = \frac{c}{2\sqrt{\varepsilon_r}}\sqrt{\left(\frac{1}{W_1}\right)^2 + \left(\frac{1}{L_1}\right)^2} \tag{2}$$

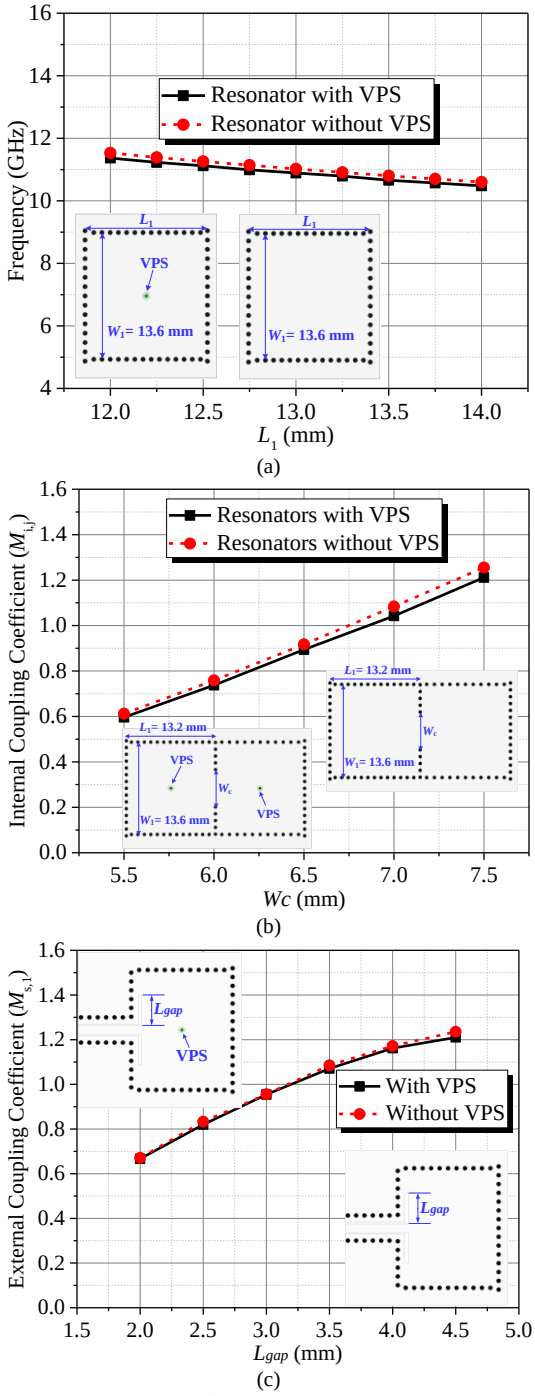

Fig. 4. Parameter extraction of resonator with/without VPS structures. (a) Resonating frequency. (b) Internal coupling coefficient ($M_{i,j}$) between two resonators. (c) External coupling coefficient ($M_{s,1}$).

$$f_{VPS} = 0.989\times f_{Normal} \quad (3)$$

The width of the inter-resonator coupling iris determines the internal coupling coefficients ($M_{i,j}$). Fig. 4(b) presents the extracted coupling coefficient versus the width of the coupling iris (W_c). It increases with W_c. Again, the presence of the VPS structure has little effect on the coupling coefficients. When W_c increases from 5.5 to 7.5 mm, the deviating of the coupling between the two cases is within 2.82%.

The external coupling coefficients ($M_{s,1}$ and $M_{L,5}$) between the external port and the resonator are extracted in Fig. 4(c).

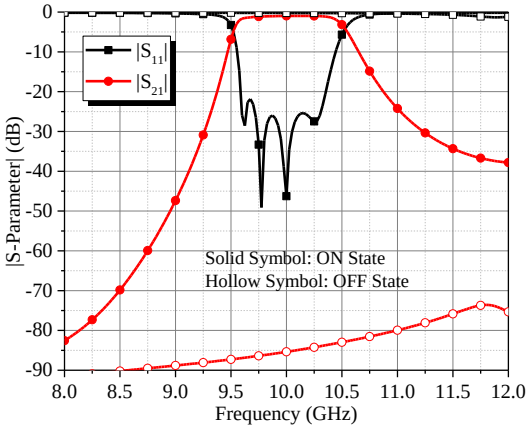

Fig. 5. Simulated results of a SPST filtering switch.

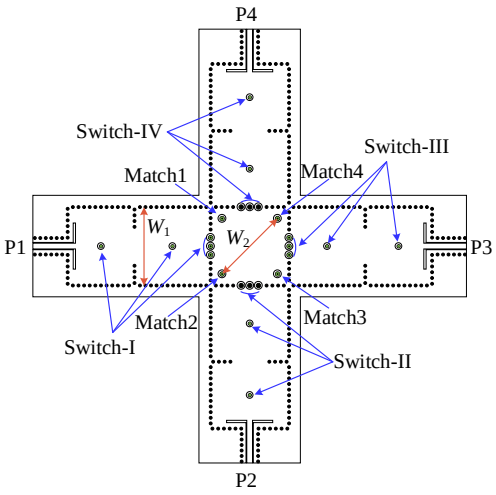

Fig. 6. Configuration of the cross-shaped SPTT filtering switch.

The coupling increases with increasing L_{gap}. With or without the VPS structure, the external coupling coefficients are barely affected.

Based on the above extracted design curves, the initial physical dimensions can be determined and a preliminary circuit prototype can be constructed. This is followed by further optimization through fine tuning before achieving the desired filtering response.

The simulated responses of the SPST filtering switch are plotted in Fig. 5. In the ON state, the reflection coefficient within the passband is below -20 dB over 9.6 - 10.37 GHz (9.71%). The minimum IL is 0.95 dB, and the suppression levels at 8 and 12 GHz are -82 and -38 dB, respectively. In the OFF state, the isolation between port1 and port2 is higher than 84 dB over 9.5-10.5 GHz.

B. Cross-Shaped Single-Pole-Three-Throw (SPTT) Filtering Switch

As shown in Fig. 6, two crisscrossed SPST filters form the SPTT filtering switch. The paths from port 1 to ports 2, 3, and 4 are nearly the same and operate at the same frequency band. The Switch-I, -II, -III, and -IV structures are utilized to switch among the three different filtering paths, while Matchs1, 2, 3, and 4 are applied to attain impedance matching at the 90º bend when the transmitting path is from P1 to P2 or P4. The operation states of the SPTT filtering switch are listed in Table

TABLE II
OPERATIONAL STATES OF THE FILTERING SPTT SWITCH

State*	State-I	State-II	State-III
Output transmission Port	P2	P3	P4
Switch-II	ON	OFF	OFF
Switch-III	OFF	ON	OFF
Switch-IV	OFF	OFF	ON
Match3	ON	ON	OFF
Match4	OFF	ON	ON

*Note: P1 is designated as the input port, therefore Switch-I, Match1, and Match2 remain on.

II. Due to symmetry, only the simulated results of State-I (from P1 to P2) and State-II (to P3) are provided. At State-I, the Switch-III and -IV are covered by the LM to block the path to P3 and P4. The Match4 is also covered by the LM to reduce to a shorting via and enhance the matching to the transmission port P2. Its effect can be seen from Fig. 7(a), where the simulated results for this state with or without Match4 are compared. It is clear that the use of Match4 improves impedance matching at the 90º bend. Essentially, the Matchs 1-4 structures are used to compensate for the parasitic capacitance at the SIW waveguide bend. Turning the VPS into a shorting via by covering it with LM introduces a shunt inductance, which cancels the excess capacitance and improves impedance matching. At State-II, the Switch-II, and -IV are covered by the LM blocking the path to P2 and P4. P3 becomes the through port. The simulated results are shown in Fig. 7(b). The overlapped bandwidth between the two states is 9.56-10.44 GHz (FBW = 8.8%), the simulated IL is 0.95 dB at 10 GHz, the isolation level is 68 dB at 10 GHz, and the suppression level is 80 dB at 8 GHz and 40 dB at 12 GHz.

As discussed in Section II-A, the high-*k* material could also be used to switch the states of the VPS structures. To verify this, the LM in the filtering switch is replaced by distilled water (ε_r = 81) and BLT (ε_r = 200) in the simulation. As shown in Fig. 8, with distilled water, the reflection coefficient deteriorates, and the IL at 10 GHz increases from 0.95 to 1.47 dB. However, using the BLT substrate, the reflection coefficient improves, as the higher dielectric constant results in a larger equivalent shunt capacitance.

IV. DESIGN OF SWITCHPLEXER

A. Design Concept

All the three paths of the cross-shaped SPTT operate at the same frequency band. In some application, the RF system needs to be switched between different frequency bands [34], [41]. Therefore, a multiple-frequency filtering switch, also called a switchplexer, is demonstrated. Fig. 9 illustrates the proposed switchplexer, and the corresponding circuit topology. It is a T-junction multiplexer [42], [43]. All channels are connected in parallel to the input port through a common SIW waveguide. It should be noted that there is no extra half-wavelength phase shifter between the adjacent channels. Different from a multiplexer, each resonant node is switchable using the VPS structure.

The process flowchart for the proposed multiplexer is illustrated in Fig. 11, as depicted below:

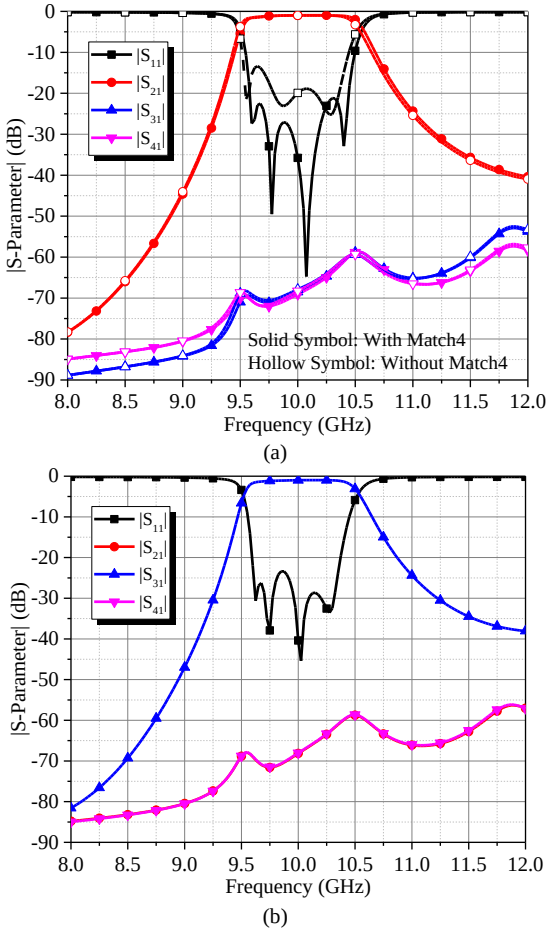

Fig. 7. Simulated results of filtering SPTT switch. (a) State-I. (b) State-II.

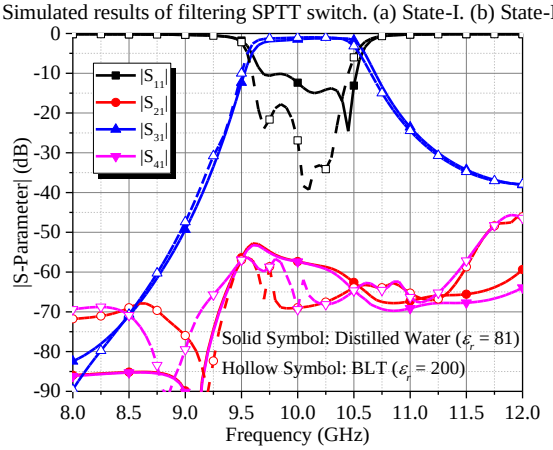

Fig. 8. Simulated results of filtering switch when LM is replaced by high-k substrate in State-II.

Step 1: Design each channel filter separately by employing the standard filter design method tailored to the specifications (e.g. the frequency band and suppression level) of each channel of the multiplexer. This work utilizes standard Chebyshev filters as an example.

To combine all channel filters together, a piecewise optimization strategy is adopted here to optimize the entire switchplexer.

Step 2: Arrange each channel in descending order based on its frequency, from high to low.

Step 3: The filter with the highest operating frequency is added to the termination of the common SIW waveguide. The

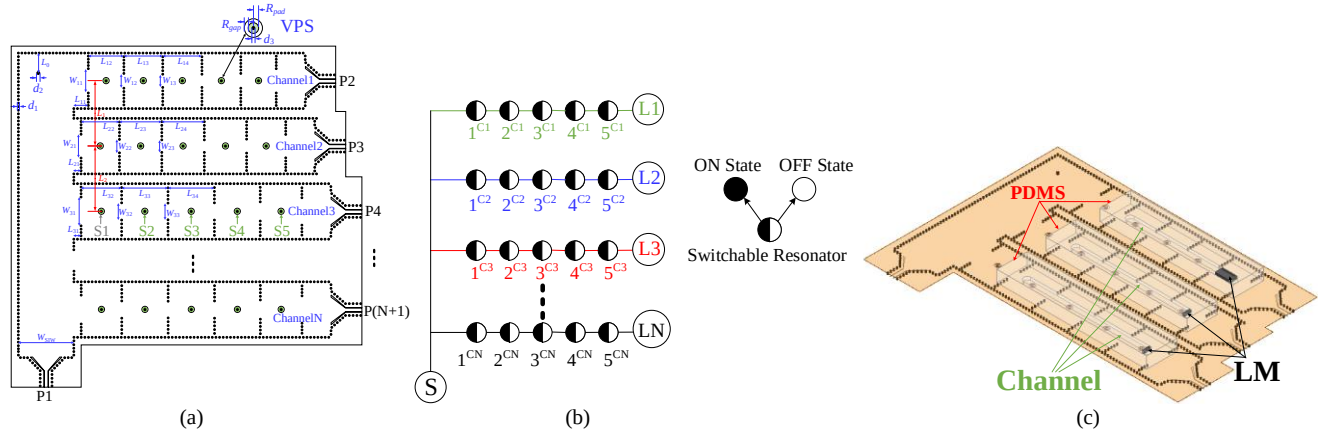

Fig. 9. Switchplexer. (a) Configuration. (b) Coupling topology. (c) 3D view of the simulated model in HFSS.

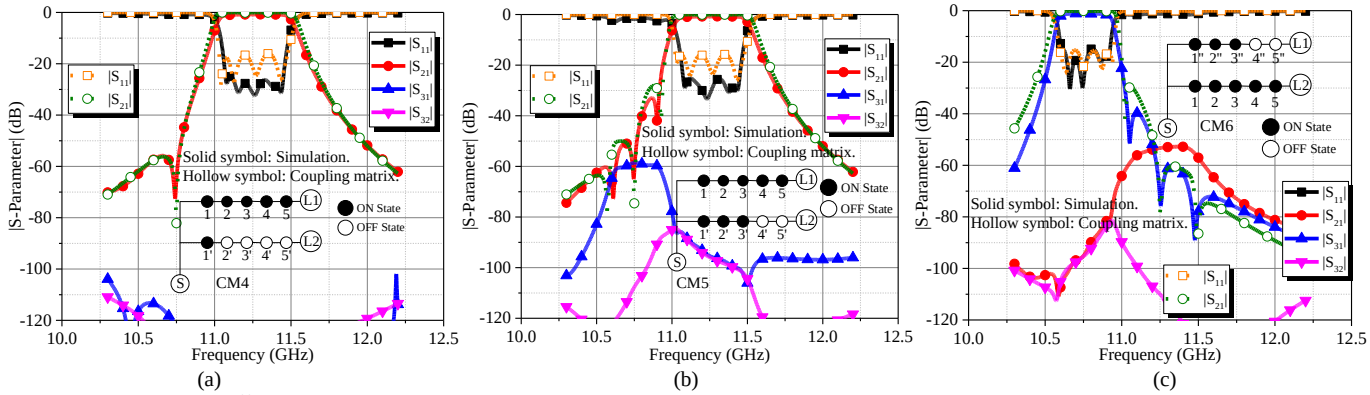

Fig. 10. Channel loading effect as seen in a two-channel switchplexer. Insets shows the coupling topology. The responses are comparison between those predicted from the synthesized coupling matrix and from simulations, when (a) S2-S5 and (b) S4-S5 in Channel2 are switched OFF; (c) S4-S5 in Channel1 are OFF.

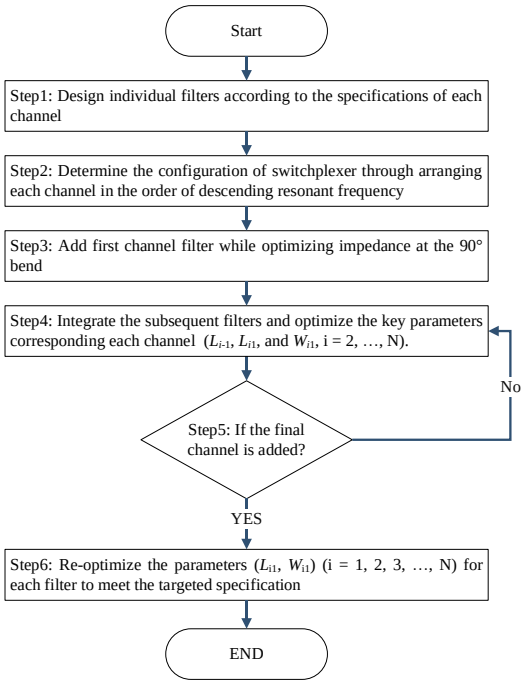

Fig. 11. Process flowchart of the proposed multiplexer.

via at the 90° bend is optimized to improve impedance matching.

Step 4: Add the subsequent channel filters into the common SIW waveguide. Optimize the phase length (L_{i-1}, i = 2, …, N) between adjacent channels, the phase length (L_{i1}) from the common SIW waveguide to first iris of the channel filter, and the width (W_{i1}) of the first iris. It should be noted that the optimization converges quickly since there are only three parameters (L_{i-1}, L_{i1}, and W_{i1}) needed.

Step 5: Repeat Step 4 to incorporate the remaining channel filters into the common SIW waveguide.

Step 6: Re-optimize the parameters (L_{i1}, W_{i1}) (i = 1, 2, 3, …, N) for each channel filter until the optimal performance of the multiplexer is achieved.

From Fig. 9, we can find every channel has five switchable VPS elements, e.g., S1, S2, S3, S4, and S5. When one VPS element is covered by the LM, the corresponding resonator is short-circuited, and the channel is partly blocked. When all five elements are covered, the channel is fully blocked. This way different channel combinations can be realized through switching ON or OFF the channels. As shown in Fig. 9(c), the liquid metals in the simulation are represented by length-adjustable cuboids of LM materials. The VPS will be switched OFF when it is covered by the LM cuboid. As the length of the LM cuboid increases, more VPS structures are covered and therefore switched OFF. Conversely, more VPS structures are switched ON when the length of the LM cuboid reduces. In addition, the microfluidic channels have been considered in the simulation.

B. Channel Loading Effect and Transmission Zeros

For the T-junction multiplexer configuration, there is mutual loading effect between channels. On the one hand, this interaction complicates the design and degrades the channel selectivity. On the other hand, this can be explored to generate

CM1

	S	1	2	3	4	5	L
S	0	1.014	0	0	0	0	0
1	1.014	0	0.865	0	0	0	0
2	0	0.865	0	0.636	0	0	0
3	0	0	0.636	0	0.636	0	0
4	0	0	0	0.636	0	0.865	0
5	0	0	0	0	0.865	0	1.014
L	0	0	0	0	0	1.014	0

(a)

CM2

	S	1'	2'	3'	4'	5'	L2
S	0	0.928	0	0	0	0	0
1'	0.928	2.34	0.725	0	0	0	0
2'	0	0.725	2.34	0.533	0	0	0
3'	0	0	0.533	2.34	0.533	0	0
4'	0	0	0	0.533	2.34	0.725	0
5'	0	0	0	0	0.725	2.34	0.928
L2	0	0	0	0	0	0.928	0

(b)

CM3

	S	1"	2"	3"	4"	5"	L1
S	0	1.107	0	0	0	0	0
1"	1.107	-2.79	1.032	0	0	0	0
2"	0	1.032	-2.79	0.759	0	0	0
3"	0	0	0.759	-2.79	0.759	0	0
4"	0	0	0	0.759	-2.79	1.032	0
5"	0	0	0	0	1.032	-2.79	1.107
L1	0	0	0	0	0	1.107	0

(c)

Fig. 12. Coupling matrices when (a) Channel1 and 2 are normalised to their respective central frequency; (b) Channel2 is renormalised to f_{01}; and (c) Channel1 is renormalised to f_{02}.

CM4

	S	1	2	3	4	5	1'	L1
S	0	1.014	0	0	0	0	0.928	0
1	1.014	-0.5	0.865	0	0	0	0	0
2	0	0.865	-0.08	0.636	0	0	0	0
3	0	0	0.636	0	0.636	0	0	0
4	0	0	0	0.636	0	0.865	0	0
5	0	0	0	0	0.865	0	0	1.014
1'	0.928	0	0	0	0	0	2.34	0
L1	0	0	0	0	0	1.014	0	0

(a)

CM5

	S	1	2	3	4	5	1'	2'	3'	L1
S	0	1.014	0	0	0	0	0.928	0	0	0
1	1.014	-0.5	0.865	0	0	0	0	0	0	0
2	0	0.865	-0.08	0.636	0	0	0	0	0	0
3	0	0	0.636	0	0.636	0	0	0	0	0
4	0	0	0	0.636	0	0.865	0	0	0	0
5	0	0	0	0	0.865	0	0	0	0	1.014
1'	0.928	0	0	0	0	0	2.34	0.725	0	0
2'	0	0	0	0	0	0	0.725	2.34	0.533	0
3'	0	0	0	0	0	0	0	0.533	2.34	0
L1	0	0	0	0	0	1.014	0	0	0	0

(b)

CM6

	S	1	2	3	4	5	1"	2"	3"	L2
S	0	1.014	0	0	0	0	1.107	0	0	0
1	1.014	0.5	0.865	0	0	0	0	0	0	0
2	0	0.865	0.1	0.636	0	0	0	0	0	0
3	0	0	0.636	0	0.636	0	0	0	0	0
4	0	0	0	0.636	0	0.865	0	0	0	0
5	0	0	0	0	0.865	0	0	0	0	1.014
1"	1.107	0	0	0	0	0	-2.79	1.032	0	0
2"	0	0	0	0	0	0	1.032	-2.79	0.759	0
3"	0	0	0	0	0	0	0	0.759	-2.79	0
L2	0	0	0	0	0	1.014	0	0	0	0

(c)

Fig. 13. Coupling matrices corresponding to the topologies in the insets of (a) Fig. 10(a); (b) Fig. 10(b); (c) Fig. 10(c). The highlighted coupling coefficients in (a) and (b) come from CM2 while those in (c) come from CM3.

TABLE III
GEOMETRIES OF THE PROPOSED SWITCHPLEXER

L_{11}	L_{12}	L_{13}	L_{14}	W_{11}	W_{12}	W_{13}	L_0	L_1	L_2	L_{21}	L_{22}	L_{23}	L_{24}	W_{SIW}
4	9.82	10.73	10.82	6.7	4.08	3.64	5.5	18	18	2	10.6	11.69	11.74	15.3
W_{21}	W_{22}	W_{23}	d_1	d_2	d_3	L_{31}	L_{32}	L_{33}	L_{34}	W_{31}	W_{32}	W_{33}	R_{gap}	R_{pad}
6.55	3.7	3.45	0.5	0.8	0.5	2	11.2	12.8	12.81	7.95	4.75	4.6	0.13	0.13

TABLE IV
OPERATIONAL STATES OF THE SWITCHPLEXER

	SPTT Filtering Switch			Switchable Diplexer			Multiplexer
	State-I	State-I	State-III	State-IV	State-V	State-VI	State-VII
Transmission Ports	P2	P3	P4	P3, P4	P2, P4	P2, P3	P2, P3, P4
S2-S5 in Channel1	ON	OFF	OFF	OFF	ON	ON	ON
S2-S5 in Channel2	OFF	ON	OFF	ON	OFF	ON	ON
S2-S5 in Channel3	OFF	Off	ON	ON	ON	OFF	ON

transmission zero (TZ) [42], [43] and improve the stopband attenuation. Herein, we will analyze the loading effect, aiming to utilize the TZ features through the proposed VPS structure.

A two-channel switchplexer is used and simulated as an example to show the control of the TZs through channel loading. The inset of Fig. 10 illustrates three circuit topologies that give different TZs distributions. In Fig. 10(a), Channel1 (f_{01} = 11.25 GHz, BW_1 = 0.45 GHz) is switched on, while all but resonator 1' are turned OFF in Channel2 (f_{02} = 10.75 GHz, BW_2 = 0.34 GHz). This residual resonator 1', loaded to Channel 1, provides a TZ in its lower stopband as shown in the simulation. In Fig. 10(b), three resonators in Channel 2 are kept ON. It is clear that three TZs are produced in the lower stopband. In Fig. 10(c), Channel2 is turned ON while two of the five resonators in Channel1 are switched OFF. The three residual resonators, loaded to Channel2, produce three clear TZs in its upper stopband. This shows that the number of TZs can be controlled by the number of kept-on resonator nodes in the switched-OFF channel. It has to be said that the location of the TZs is not readily controllable just by the two-bit ON/OFF control of the resonators. However, if the resonators are tunable in frequency, the locations of the TZs will become tunable too.

Next, we will show that the TZs can be synthesized theoretically using coupling matrix. Fig. 12(a) gives the coupling matrix (CM1) for both channels normalized to their respective central frequencies, f_{01} and f_{02}. If we consider Channel1 as the primary signal route at f_{01}, Channel2 can be treated as a shunt asynchronously-tuned filter. Its coupling matrix at f_{01} can be extracted when its response is renormalized to f_{01}. This becomes CM2, as given in Fig. 12(b), a matrix that approximates the loading effect of Channel2 on Channel1. Now consider Channel2 as the primary signal route at f_{02}. Similarly, Fig. 12(c) shows the extracted coupling matrix (CM3) for Channel1 when its response is renormalized to f_{02}. This represents its loading effect on Channel2.

Looking at the circuit topology in Fig. 10(a) again, it can be represented, as a first-order approximation, by a coupling matrix that contains all the resonators in Channel1, the one residual resonator 1' in Channel2 and the associated mutual couplings. Specifically, the self-coupling of resonator 1' and its coupling to the source can be taken from CM2 given in Fig. 12(b). Additionally, the coupling between resonator 1 and 1' is ignored due to the high isolation between two channels. These are highlighted in green color in the resultant CM4 in Fig. 13(a). The response corresponding to CM4 agrees very well with the simulation in Fig. 10(a). The position of the TZ (10.75 GHz) is accurately predicted by the constructed coupling matrix.

The same method can be applied to the cases in Fig. 10(b) and (c). In Fig. 10(b), three shunt-connected resonators were turned ON and their couplings as loading elements are considered in CM5, given in Fig. 13(b). The three TZs predicted from the coupling matrix CM5 agree with the simulation very well (10.56, 10.75, and 10.95 GHz). Similarly, the topology in Fig. 10(c) can be represented by CM6 in Fig.

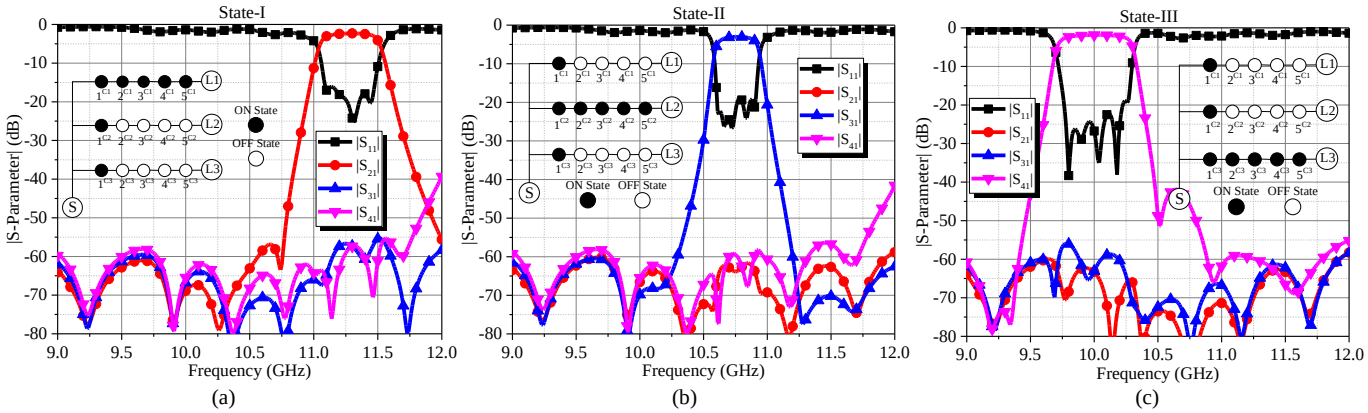

Fig. 14. Operation Case I of the switchplexer as switchable filters when two channels are switched OFF. (a) Channel2 and Channel3 are switched OFF (State-I). (b) Channel1 and Channel3 are OFF (State-II). (c) Channel1 and Channel2 are OFF (State-III).

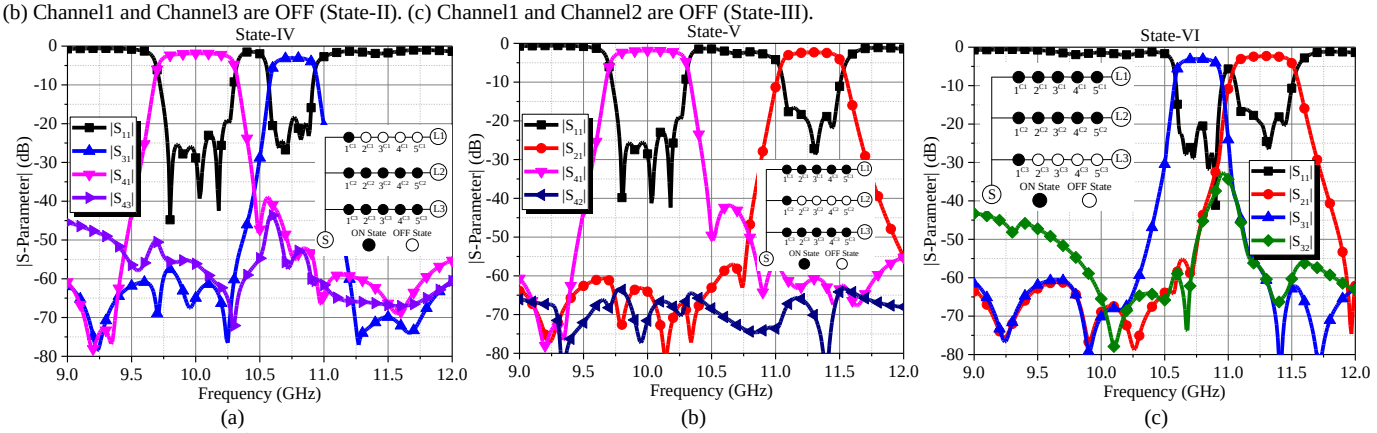

Fig. 15. Operation Case II of the switchplexer as switchable diplexers when only one channel is switched OFF. (a) Channel1 (State-IV), (b) Channel2 (State-V), and (c) Channel3 (State-VI) are switched OFF, respectively.

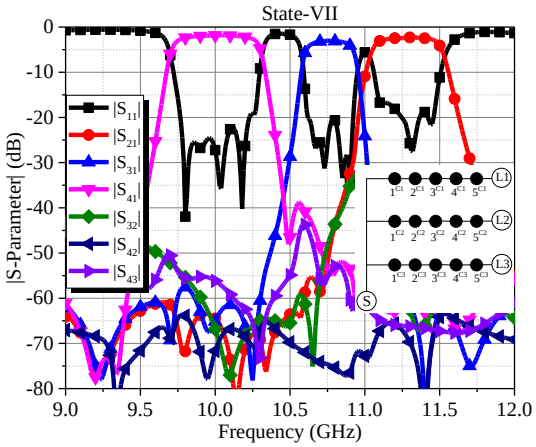

Fig. 16. Simulated results of Case III as a triplexer.

13(c), and three TZs were generated at higher stopband. It can be seen that the reciprocal loading effect from the channel filter can be utilized to produce transmission zeros by switching ON/OFF resonators through the proposed VPS structure. This feature was also used in the next three-channel switchplexer design to improve the channel performance.

C. Three-Channel Switchplexer

A switchplexer with three channels are demonstrated here. The bandwidths for the three channels are 11.05-11.5 GHz, 10.55-10.9 GHz, and 9.7-10.3 GHz, respectively. All channels are set to be 5th-order Chebyshev response as before. The key dimensions of the switchplexer after optimization are given in Table III.

(1) Case I: Switchable channel filter

Only one channel is switched ON at a time. Fig. 14 shows the simulated responses of the three states and the corresponding coupling topology (inset). In this example, the first resonator node (next to the T-junction) of each of the two switched-OFF channels is kept ON. As discussed in Section IV-B, this will provide TZs to the ON channel so as to improve its channel selectivity. The simulated insertion losses are 2.3 (Channel1), 3.08 (Channel2), and 1.84 dB (Channel3), respectively. The bandwidths are 11.04-11.49, 10.57-10.91, and 9.72-10.3 GHz. All rejections are greater than 50 dB at the switched-OFF channel.

(2) Case II: Switchable diplexer

Two of the three channels can be switched ON and the channel combinations can be reconfigured. Fig. 15 shows the simulated results of three different diplexer states. Their bandwidths show a good consistency with the one-channel operation state in Case I. All simulated isolations between the two channels are greater than 33 dB.

(3) Case III: Triplexer

All three channels are switched ON. It works as a triplexer. Fig. 16 shows the simulated results. The bandwidths are 11.04-11.54, 10.56-10.93, and 9.72-10.3 GHz, respectively, and the corresponding insertion losses are 2.3, 3.1, and 1.85 dB. All isolations are greater than 30 dB. The variation of the ILs is mainly attributed to the different bandwidths of the channels. It should be noted that more loading resonant nodes

can be added in parallel to improve the channel selectivity, if needed.

V. Prototype and Measurement

As shown in Fig. 17, the cross-shaped filtering switch and the three-channel switchplexer are fabricated by PCB technology. The microfluidic channels that contain the LM are fabricated from PDMS [20]. The PCB and the microfluidic channels are bonded together by plasma bonding method. For demonstration purpose, the LM is actuated by using peristaltic pumps to switch ON and OFF the VPS structures. Firstly, the LM is injected in the microfluidic channels, and mineral oil is pumped into the tubes. We use this oil to seal and push the LM. Then, the peristaltic pump and microfluidic channels are connected by tubes. By rotating the pump in one direction or the other, the LM is can be moved to cover and empty from the VPSs. It should be noted that these external structures (PDMS channels, tunes, and pumps) have little effect on the circuits because of the natural shielding effect of the SIW structures.

The measured results of the cross-shaped SPTT filtering switch are shown Fig. 18. Each of the three paths can be switched ON. The overlapped bandwidth is 9.56-10.44 GHz (FBW = 8.8%), the measured IL is about 1.55 dB at 10 GHz, the out-of-band suppression is better than 40 dB at 8 and 12 GHz, and the isolation is better than 58 dB at 10 GHz. The measured results agree well with the simulations except for a minor increase in IL and a slightly reduced isolation of 5 dB. To demonstrate that the VPS structures can be switched not only by LM but also by high-k material, distilled water is utilized to tune the filtering switch. The measured results are also shown in Fig. 18. The switching effect is clear, but the

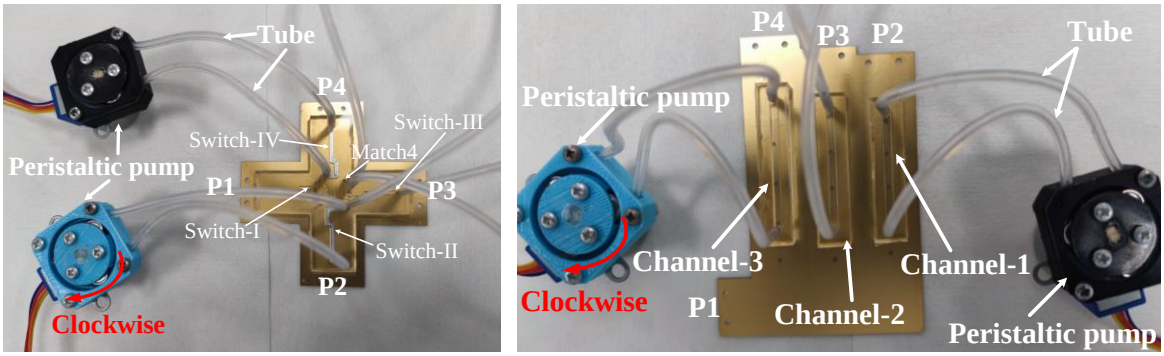

(a) (b)

Fig. 17. Prototype devices. (a) Cross-shaped SPTT filtering switch. (b) Switchplexer.

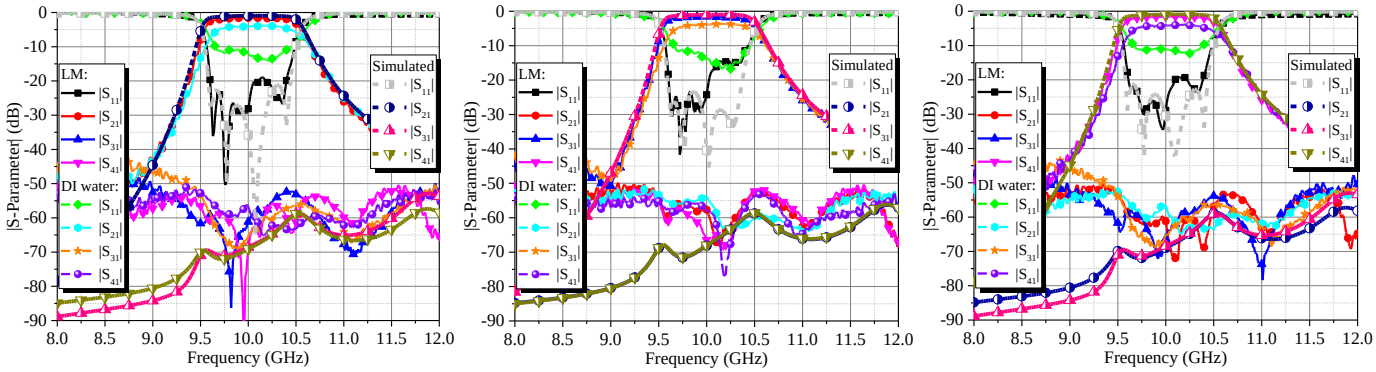

(a) (b) (c)

Fig. 18. Measured results of the cross-shaped SPTT filtering switch when (a) P2, (b) P3, and (c) P4 are switched ON, respectively.

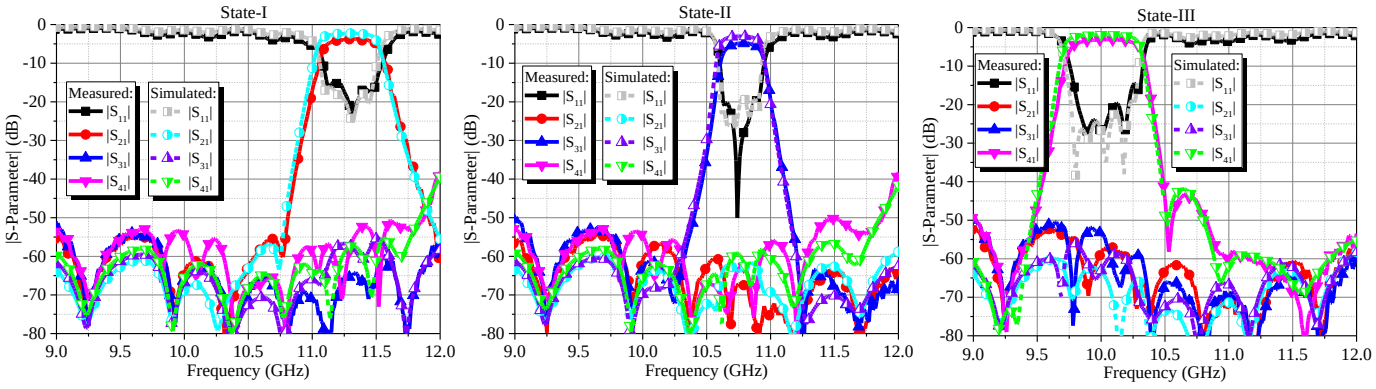

(a) (b) (c)

Fig. 19. Measured results of the switchplexer as switchable filters (Case I). (a) P2 (State-I), P3 (State-II), and P4 (State-III) are switched ON, respectively.

TABLE V
COMPARISON OF REPORTED FILTERING SWITCHES

	10-*dB FBW*		*Type*	f_0 (*GHz*)	*IL* (*dB*)	*Suppression level* (*dB*)	*Isolation level* (*dB*)	*Structure*	*Size and Material*	*Order*
[30]	9% (3-dB FBW)		SPST	0.9	3	20	44	Microstrip line+ P-I-N diode	$0.31\times0.28\lambda_g^2$, RO4003C	2
[31]	9% (3-dB FBW)		SPDT	0.78	1.8	20	28	Microstrip line+ P-I-N diode	$0.081\times0.074\lambda_g^2$, RO4003	2
[32]	10%		SPDT	1	0.97	20	20	Multicoupled line+P-I-N diode	$0.158\times0.17\lambda_g^2$, RO4350B	3
[33]	5% (3-dB FBW)		SPDT	1.49	3.6	30	47	Microstrip line+ P-I-N diode	$0.45\times0.3\lambda_g^2$, RO4003	4
[34]	~2.85% (1-dB FBW)		SPDT	1.65-1.84	6.73	32.5	40	Microstrip line+ Varactor	$0.24\times0.42\lambda_g^2$, Rogers 6010	4
[35]	11.1% (3-dB FBW)		SP4T	0.99	1.76	38	45.7	Microstrip line+ P-I-N diode	$0.28\times0.32\lambda_g^2$, Rogers 5880	3
[36]	3.8% (3-dB FBW)		SPDT	1.953-2.782	3.11	45	47	SIW+Varactor+Piezo	$0.47\times0.41\ \lambda_g^2$, Rogers 4350B	3
This Work	**8.8%**		**SPTT**	**10**	**1.55**	**40**	**58**	**SIW+LM**	**$3.7\times3.7\lambda_g^2$, TLY-5**	**5**
	Channel1	**4.15%**	**Switchplexer**	**11.32**	**3.76**	**50**	**50**	**SIW+LM**	**$3.31\times4.78\lambda_g^2$ TLY-5**	**5**
	Channel2	**3.52%**		**10.8**	**4.78**					
	Channel3	**5.67%**		**10**	**2.98**					

Note: λ_g is the wavelength at f_0.

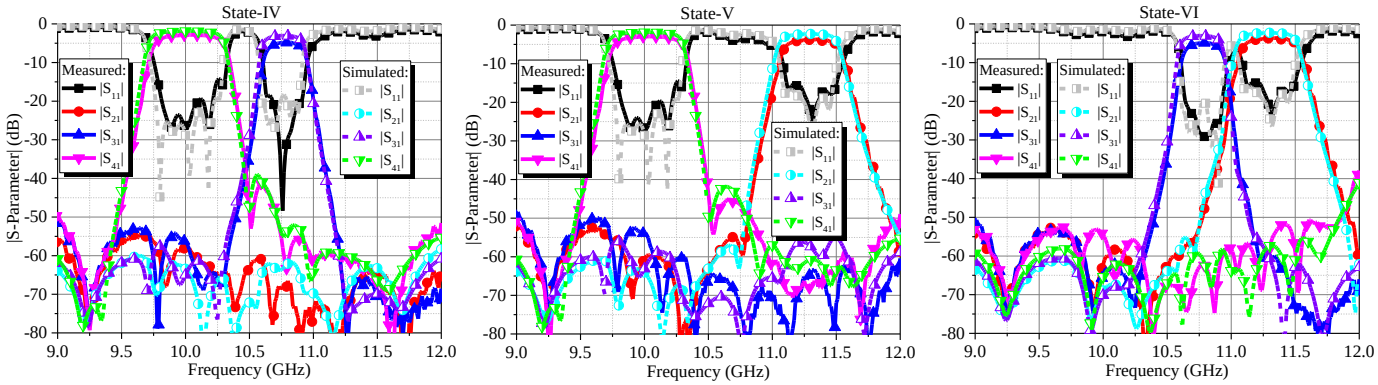

Fig. 20. Measured results of the switchplexer as switchable diplexers (Case II). (a) P2 (State-IV), (b) P3 (State-V), and (c) P4 (State-VI) are switched OFF, respectively.

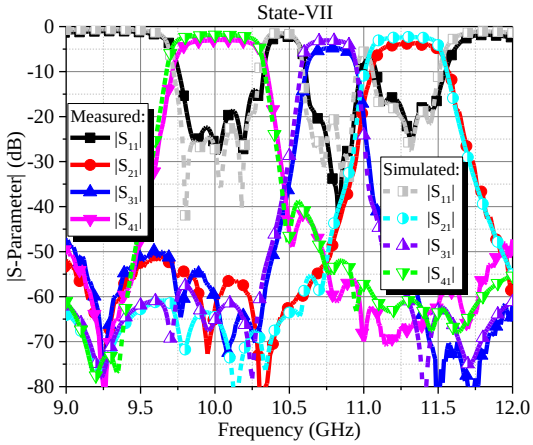

Fig. 21. Measured results of the switchplexer as a triplexer (Case III).

reflection coefficient deteriorates by 12.5 dB, and the overlapped passband bandwidth is 9.65-10.46 GHz (10%). The IL increases to 3.83 dB at 10 GHz. Common aqueous solutions such as water and seawater act as conductors and would improve the reflection coefficients of the devices. The suppression and isolation level keep almost the same.

The measured results of the switchplexer are presented in Figs. 17- 19. Fig. 19 shows the Case I operation as switchable channel filters. Each port can be switched ON individually while the other two ports are OFF. The filtering properties of each channel keep well, and the isolation levels are better than 50 dB in the operating bandwidths. From Fig. 19(b), it is evident that several TZs are generated in both lower and upper stopbands because of the resonant loading as discussed previously. Fig. 20 shows the Case II operation as switchable diplexers, when one of the channels is switched OFF by covering S2-S5 with the LM, while the other two keep operating. The isolation and suppression levels remain high. Fig. 21 shows the Case III operation as a triplexer, when all the channels are switched ON. The channel bandwidths are 11.08-11.55 GHz, 10.61-10.99 GHz, and 9.76-10.33 GHz, respectively. The corresponding insertion losses at three channels are 3.76, 4.78, and 2.98 dB, respectively. The isolation levels are better than 50 dB in the passbands, and the suppression levels are better than 50 dB at 9 and 12 GHz. The proposed SPTT filtering switch is compared with the other P-I-N based SPST/SPDT filtering switches in Table V.

Compared with the proposed SPTT filtering switch, most of these switches operates at lower frequency with relatively high insertion loss [30], [31], [33], [34], [35], [36]. In addition, the proposed filtering switches have shown higher suppression and isolation levels. It should be noted that the switching time for P-I-N and varactor diodes is in the nanosecond to microsecond range, whereas the switching time for the LM-based filtering switch is in the millisecond to second range.

VI. Conclusion

Using a liquid-metal-enabled VPS structure, an X-band cross-shaped SPTT filtering switch and a switchplexer are presented. As the LM only flows on the surface of the SIW, the losses introduced by the LM are minimal. This switching structure also simplifies the fabrication of the microfluidic channels and the actuation of the LM. The cross-shaped SPTT filtering switch has shown an excellent suppression level of 40 dB at 10 GHz and isolation level of 58 dB. In addition, the impedance matching is significantly improved due to the use of additional matching VPSs at the 90° bend. As for the switchplexer, it can flexibly switch in and out one or more channels without affecting the others. It has also been shown that the number of the TZs can be flexibly controlled by exploring the loading effect of the switched-OFF channel, which improves the rejection of the filter. Moreover, we have also shown that high-*k* materials, such as water and BLT, can also be utilized to switch the VPS structures. It is anticipated that the VPS based switching element can be integrated with other devices for multifunctional circuits and systems.

References

[1] T. Yang and G. M. Rebeiz, "Bandpass-to-bandstop reconfigurable tunable filters with frequency and bandwidth controls," *IEEE Trans. Microw. Theory Techn.*, vol. 65. no. 7, pp: 2288-2297, 2017. DOI: 10.1109/tmtt.2017.2679182.

[2] M.-L. Chuang and M.-T. Wu, "Microstrip multiplexer and switchable diplexer with joint t-shaped resonators," *IEEE Microwave Wireless Compon. Lett.*, vol. 24. no. 5, pp: 309-311, 2014. DOI: 10.1109/lmwc.2014.2309084.

[3] S. Bahrami, G. Moloudian, H.-J. Song, and J. L. Buckley, "Reconfigurable uwb circularly polarized slot antenna with three modes of operation and continuous tuning rang," *IEEE Trans. Antennas Propag.*, vol. 70. no. 9, pp: 8542-8547, 2022. DOI: 10.1109/tap.2022.3161358.

[4] G. M. Rebeiz, C. D. Patel, S. K. Han, K. Chih-Hsiang, and K. M. J. Ho, "The search for a reliable mems switch," *IEEE Microwave Mag.*, vol. 14. no. 1, pp: 57-67, 2013. DOI: 10.1109/mmm.2012.2226540.

[5] X. Tan and Y. Zhang, "Tunable couplers: An overview of recently developed couplers with tunable functions," *IEEE Microwave Mag.*, vol. 24. no. 3, pp: 20-33, 2023. DOI: 10.1109/mmm.2022.3226550.

[6] F. Wu and K. M. Luk, "Single-port reconfigurable magneto-electric dipole antenna with quad-polarization diversity," *IEEE Trans. Antennas Propag.*, vol. 65. no. 5, pp: 2289-2296, 2017. DOI: 10.1109/tap.2017.2681437.

[7] W. Lin, S.-L. Chen, R. W. Ziolkowski, and Y. J. Guo, "Reconfigurable, wideband, low-profile, circularly polarized antenna and array enabled by an artificial magnetic conductor ground," *IEEE Trans. Antennas Propag.*, vol. 66. no. 3, pp: 1564-1569, 2018. DOI: 10.1109/tap.2018.2790437.

[8] M. Li, Z. Zhang, M.-C. Tang, L. Zhu, and N.-W. Liu, "Bandwidth enhancement and size reduction of a low-profile polarization-reconfigurable antenna by utilizing multiple resonances," *IEEE Trans. Antennas Propag.*, vol. 70. no. 2, pp: 1517-1522, 2022. DOI: 10.1109/tap.2021.3111309.

[9] S. Bulja and A. Grebennikov, "Variable reflection-type attenuators based on varactor diodes," *IEEE Trans. Microw. Theory Techn.*, vol. 60. no. 12, pp: 3719-3727, 2012. DOI: 10.1109/tmtt.2012.2216895.

[10] J. Ni and J. Hong, "Compact varactor-tuned microstrip high-pass filter with a quasi-elliptic function response," *IEEE Trans. Microw. Theory Techn.*, vol. 61. no. 11, pp: 3853-3859, 2013. DOI: 10.1109/tmtt.2013.2281964.

[11] X.-G. Wang, Y.-H. Cho, and S.-W. Yun, "A tunable combline bandpass filter loaded with series resonator," *IEEE Trans. Microw. Theory Techn.*, vol. 60. no. 6, pp: 1569-1576, 2012. DOI: 10.1109/tmtt.2012.2189123.

[12] M. Zhou, et al., "A varactor based 90° directional coupler with tunable coupling ratios and reconfigurable responses," *IEEE Trans. Microw. Theory Techn.*, vol. 62. no. 3, pp: 416-421, 2014. DOI: 10.1109/tmtt.2014.2299522.

[13] F. Huang, S. Fouladi, and R. R. Mansour, "High-q tunable dielectric resonator filters using mems technology," *IEEE Trans. Microw. Theory Techn.*, vol. 59. no. 12, pp: 3401-3409, 2011. DOI: 10.1109/tmtt.2011.2171984.

[14] C.-H. Ko, K. M. J. Ho, and G. M. Rebeiz, "An electronically-scanned 1.8–2.1 ghz base-station antenna using packaged high-reliability rf mems phase shifters," *IEEE Trans. Microw. Theory Techn.*, vol. 61. no. 2, pp: 979-985, 2013. DOI: 10.1109/tmtt.2012.2231698.

[15] S. Gong, H. Shen, and N. S. Barker, "A 60-ghz 2-bit switched-line phase shifter using sp4t rf-mems switches," *IEEE Trans. Microw. Theory Techn.*, vol. 59. no. 4, pp: 894-900, 2011. DOI: 10.1109/tmtt.2011.2112374.

[16] M. Unlu, S. Demir, and T. Akin, "A 15-40-ghz frequency reconfigurable rf mems phase shifter," *IEEE Trans. Microw. Theory Techn.*, vol. 61. no. 8, pp: 2865-2877, 2013. DOI: 10.1109/tmtt.2013.2271995.

[17] H. Zareie and G. M. Rebeiz, "Compact high-power spst and sp4t rf mems metal-contact switches," *IEEE Trans. Microw. Theory Techn.*, vol. 62. no. 2, pp: 297-305, 2014. DOI: 10.1109/tmtt.2013.2296749.

[18] T. Cole and S.-Y. Tang, "Liquid metals as soft electromechanical actuators," *Mater. Adv.*, 2022. DOI: 10.1039/d1ma00885d.

[19] Y.-W. Wu, S. Alkaraki, S.-Y. Tang, Y. Wang, and J. R. Kelly, "Circuits and antennas incorporating gallium-based liquid metal," *Proc. IEEE*, vol. 111. no. 8, pp: 955-977, August, 2023. DOI: 10.1109/jproc.2023.3285400.

[20] Y.-W. Wu, S.-Y. Tang, J. Churm, and Y. Wang, "Liquid metal-based tunable linear phase shifters with low insertion loss, high phase resolution, and low dispersion," *IEEE Trans. Microw. Theory Techn.*, vol. 71. no. 9, pp: 3968-3978, 2023. DOI: 10.1109/tmtt.2023.3248954.

[21] C.-H. Chen, J. Whalen, and D. Peroulis, "Non-toxic liquid-metal 2-100 ghz mems switch," in *2007 IEEE/MTT-S International Microwave Symposium*, Honolulu, HI, USA, IEEE, 2007. DOI: 10.1109/MWSYM.2007.380446.

[22] M. R. Moorefield, R. C. Gough, A. T. Ohta, and W. A. Shiroma, "An electrically actuated dc-to-11-ghz liquid-metal switch," *IEEE Access*, vol. 6. pp: 1261-1266, 2018. DOI: 10.1109/access.2017.2778184.

[23] P. Sen and K. Chang-Jin, "A liquid–solid direct contact low-loss rf micro switch," *J. Microelectromech. Syst.*, vol. 18. no. 5, pp: 990-997, 2009. DOI: 10.1109/jmems.2009.2029170.

[24] P. Sen and K. Chang-Jin, "A fast liquid-metal droplet microswitch using ewod-driven contact-line sliding," *J. Microelectromech. Syst.*, vol. 18. no. 1, pp: 174-185, 2009. DOI: 10.1109/jmems.2008.2008624.

[25] N. Vahabisani, S. Khan, and M. Daneshmand, "A k-band reflective waveguide switch using liquid metal," *IEEE Antennas Wireless Propag. Lett.*, pp: 1-1, 2017. DOI: 10.1109/lawp.2017.2679072.

[26] S. Alkaraki, J. Kelly, A. L. Borja, R. Mittra, and Y. Wang, "Gallium-based liquid metal substrate integrated waveguide switches," *IEEE Microwave Wireless Compon. Lett.*, vol. 31. no. 3, pp: 257-260, 2021. DOI: 10.1109/lmwc.2020.3040795.

[27] J.-X. Xu and X. Y. Zhang, "Single- and dual-band ltcc filtering switch with high isolation based on coupling control," *IEEE Trans. Ind. Electron.*, vol. 64. no. 4, pp: 3137-3146, 2017. DOI: 10.1109/tie.2016.2633534.

[28] P. Sun, P. Upadhyaya, D.-H. Jeong, D. Heo, and G. S. La Rue, "A novel sige pin diode spst switch for broadband t/r module," *IEEE Microwave Wireless Compon. Lett.*, vol. 17. no. 5, pp: 352-354, 2007. DOI: 10.1109/lmwc.2007.895706.

[29] Z.-C. Hao, W.-Q. Ding, and W. Hong, "Developing low-cost w-band siw bandpass filters using the commercially available printed-circuit-board technology," *IEEE Trans. Microw. Theory Techn.*, vol. 64. no. 6, pp: 1775-1786, 2016. DOI: 10.1109/tmtt.2016.2553029.

[30] W.-H. Tu, "Switchable microstrip bandpass filters with reconfigurable on-state frequency responses," *IEEE Microwave Wireless Compon. Lett.*, vol. 20. no. 5, pp: 259-261, 2010. DOI: 10.1109/lmwc.2010.2045581.
[31] J.-X. Xu, X. Y. Zhang, and Y.-M. Xue, "Compact filtering switch with wide-stopband response," *IEEE Access*, vol. 5. pp: 23803-23808, 2017. DOI: 10.1109/access.2017.2768098.
[32] C.-S. Chen, J.-F. Wu, and Y.-S. Lin, "Compact single-pole-double-throw switchable bandpass filter based on multicoupled line," *IEEE Microwave Wireless Compon. Lett.*, vol. 24. no. 2, pp: 87-89, 2014. DOI: 10.1109/lmwc.2013.2290212.
[33] S.-F. Chao, C.-H. Wu, Z.-M. Tsai, H. Wang, and C. H. Chen, "Electronically switchable bandpass filters using loaded stepped-impedance resonators," *IEEE Trans. Microw. Theory Techn.*, vol. 54. no. 12, pp: 4193-4201, 2006. DOI: 10.1109/tmtt.2006.885898.
[34] J. Lai, T. Yang, P.-L. Chi, and R. Xu, "1.866–2.782-ghz reconfigurable filtering single-pole-multithrow switches based on evanescent-mode cavity resonators," *IEEE Trans. Microw. Theory Techn.*, vol. 69. no. 2, pp: 1355-1364, 2021. DOI: 10.1109/tmtt.2020.3039960.
[35] Z. Wei, P.-L. Chi, R. Xu, and T. Yang, "A 1.65 to 1.84 ghz filtering spdt switch with fully tunable insertion phase using nrn and mixed electromagnetic coupling techniques," *IEEE Trans. Circuits Syst. II Express Briefs*, vol. 70. no. 9, pp: 3353-3357, 2023. DOI: 10.1109/tcsii.2023.3265005.
[36] J. Xu, Q.-H. Cai, Y.-F. Guo, S.-Y. Ji, and Y.-W. Duan, "A bpf integrated sp4t switch using parallel switched fractal common feeding line," *IEEE Trans. Circuits Syst. II Express Briefs*, vol. 68. no. 6, pp: 1932-1936, 2021. DOI: 10.1109/tcsii.2020.3048350.
[37] J. O. Garcia, J. C. Melgarejo Lermas, V. E. Boria, and M. Guglielmi, "On the integration of microwave filters and waveguide switches," *IEEE Microwave Wireless Compon. Lett.*, vol. 31. no. 3, pp: 265-268, 2021. DOI: 10.1109/lmwc.2020.3044730.
[38] S. Alkaraki, A. L. Borja, J. R. Kelly, R. Mittra, and Y. Gao, "Reconfigurable liquid metal-based siw phase shifter," *IEEE Trans. Microw. Theory Techn.*, vol. 70. no. 1, pp: 323-333, 2022. DOI: 10.1109/tmtt.2021.3124797.
[39] Z. Rahimian Omam, et al., "Tunable substrate integrated waveguide phase shifter using high dielectric constant slab," *IEEE Microwave Wireless Compon. Lett.*, vol. 30. no. 5, pp: 485-488, 2020. DOI: 10.1109/lmwc.2020.2980264.
[40] J.-S. G. Hong and M. J. Lancaster, *Microstrip filters for rf/microwave applications*. 2001: Wiley.
[41] I. C. Reines, et al., "A low loss rf mems ku-band integrated switched filter bank," *IEEE Microwave Wireless Compon. Lett.*, vol. 15. no. 2, pp: 74-76, 2005. DOI: 10.1109/lmwc.2004.842823.
[42] G. Macchiarella and S. Tamiazzo, "Synthesis of star-junction multiplexers," *IEEE Trans. Microw. Theory Techn.*, 2010. DOI: 10.1109/tmtt.2010.2086570.
[43] J. C. Melgarejo, S. Cogollos, M. Guglielmi, and V. E. Boria, "A new family of multiband waveguide filters based on a folded topology," *IEEE Trans. Microw. Theory Techn.*, vol. 68. no. 7, pp: 2590-2600, July, 2020. DOI: 10.1109/tmtt.2020.2989111.